Applied Multi-Dimensional Fusion

(A. Mahmood, P. Tudor)[♠], *W. Oxford*[♦], *R. Hansford*[♣]
(J. Nelson, N. Kingsbury)[*], *(A. Katartzis, M. Petrou, N. Mitniadous, T. Stathaki)*[*], *(A. Achim, A. Loza)*[+]

Introduction

Within the context of the Data and Information Fusion Defence Technology Centre Multi-Dimensional Fusion refers to the fusion of data and information that span several bands, more than one dimension and more than one mode of sensing.

The Applied Multi-Dimensional Fusion (AMDF) project has been developed to showcase key research in single and multi-modal data fusion, image enhancement, feature detection, tracking and fusion metrics. The aim is to hone this research into practical applicable products through the technical expertise of the commercial partners and scientific excellence of the academic partners.

In order to demonstrate the applicability of academic multi-dimensional fusion research to a military customer the project has constructed research activities around an urban surveillance, target acquisition and tracking scenario. For this purpose, the commercial partners have produced a simulated scenario that represents and highlights common issues within this challenging environment.

The scenario focuses on the detection of a known target moving through complex terrain (an urban environment) using 'video' imagery in both visible and thermal bands. It is representative of the support of an intelligence led operation where multiple air and ground based surveillance assets may be used to detect and confirm a known target within an Area of Interest derived from existing intelligence.

The scenario uses hypothetical linked assets of a type that might be used to provide the capability described in the near future. Hidden within the detail of the scenarios are many 'real-world' issues; truncated meta data, cumulative errors in sensor location and attitude determination, and changing environmental conditions.

This paper presents highlights of the work done in the area of dual-band video fusion: Effects of resolution, restoration and reconstruction of blurred data, and multi-sensor fusion on target detection, identification and tracking. The paper is presents issues in a sequential manner, though the research work is done in parallel streams. The paper starts with issues of multi-sensor scenario generation and presents a précis of scientific research conducted in the area of super resolution, fusion, tracking, and concludes with the discussion on metrics and utility of metrics to video fusion, and presents the scope of the future work in the area of utilisation of hyperspectral data.

Dual Band Video Scenario Generation

GD-UK and QinetiQ produce synthetic visible and thermal video data at High Definition (as defined by the NATO standard STANAG 4609 "Digital Motion Imagery"). These data are also down-sampled to conventional Standard Definition resolution to match current generation equipments.

The visible simulation for the scenario is developed by GD using the NewTek Lightwave 3D computer animation package, QinetiQ provides the corresponding long-wave IR imagery using its Cameosim multi-spectral simulation system. This necessitates importing scene geometry and motion data,, provided by GD, and assigning appropriate materials, and hence thermal properties, to the objects in the scene.

The scene data are provided in the form of Lightwave scene and model files. As Cameosim has no facility to import data directly from Lightwave into its own proprietary format, the conversion is performed using a two step process. The data are first converted to the OpenFlight[1] (*.flt) format that is further converted into the Cameosim format. The second task involves significantly more work than the first. Unlike 'visible' ray tracers like the one used by Lightwave, which use RGB image textures to determine the colours of objects, Cameosim

[♠] General Dynamics United Kingdom Limited, Hastings – corresponding author asher.mahmood@generaldynamics.uk.com
[♦] Waterfall Solutions Limited, Farnborough
[♣] QinetiQ, Farnborough
[*] Cambridge University, Cambridge
[*] Imperial College, London
[+] University of Bristol, Bristol

requires the use of spectral signature data, where the amount of light reflected back at each frequency is defined. These signatures allow Cameosim to render objects in a more realistic fashion and at wavelengths beyond the visible band. The down side is that collecting these data is considerably harder than creating RGB textures.

To render thermal imagery Cameosim needs the 'thermal properties' of each object to be defined, as well as the spectral signatures. This consists of defining one or more layers of different materials by defining appropriate data (density, thermal conductivity etc) for each substance. As an example, a typical cavity wall would consist of a layer of 'bricks' followed by a layer of 'insulation' then a layer of 'breeze blocks'. Together with the spectral signature, these two sets of data form a 'material', which can then be assigned to objects directly, or combined together to form textures in much the same way as the RGB textures used by 'visible' ray tracers.

One of the most technically challenging problems in generating the scene was rendering the smoke from the fire. A wide range of methods were considered, ranging from a full particle simulation to a simple post-process effect. The primary constraints were making the smoke match the smoke in the visible image while also looking realistic, and keeping the setup and rendering times to a minimum. The method chosen was to create the smoke cloud using a set of small billboard-style discs, each having a semi-transparent texture. These discs were arranged in rough layers which were moved around to emulate the smoke drifting across the scene.

Unfortunately conversion process introduced errors which were not detected until the imagery had been rendered and both versions (visible and IR) were compared. These errors were compounded (and obscured) by differences in the routes taken by the moving objects in the two rendered scenes, itself caused by the two packages using different algorithms for interpolating ('tweening') the motion information. This was resolved by extracting frame-by-frame position information for every object from the Lightwave scene and then importing those data into Cameosim.

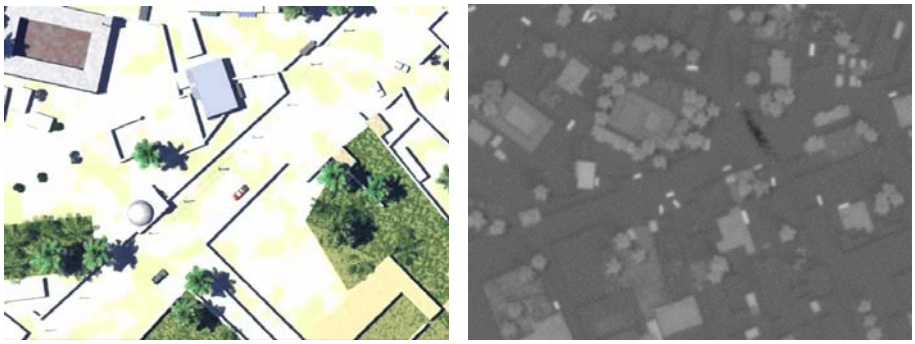

Figure 1: Visual and LWIR Data

Super resolution

Super-resolution (SR) image reconstruction is a multiframe fusion process capable of reconstructing a high resolution (HR) image from several low resolution (LR) images of the same scene. It extends classical single frame image restoration methods by simultaneously utilizing information from multiple observed images to achieve restoration at resolutions higher than that of the original data.

Imperial College is presenting a new approach that circumvents, to some degree; some of the limitations previously associated with these techniques and can be used in realistic scenarios with more complex geometric distortions (e.g. affine distortions). The SR reconstruction is formulated as a Bayesian optimization problem using a discontinuity adaptive robust kernel that characterizes the image's prior distribution. In addition, the initialization of the optimization is performed using an adapted Normalized Convolution (NC) technique [20] that incorporates the uncertainty due to mis-registration.

Imperial College has shown both qualitative and quantitative results on real video sequences and demonstrate the advantages of the proposed method compared with conventional methodologies. The general strategy that characterizes a multiframe SR process comprises three major processing steps:

a) *LR image acquisition*: acquisition of a sequence of LR images from the same scene with arbitrary geometric distortion between the images;
b) *Image registration / motion compensation*: estimation of the registration of the LR frames with each other with sub-pixel accuracy;
c) *HR image construction*: construction of a HR image from the co-registered LR images.

To start with, a look at the general formulation of the SR problem. First, an observation model relating the LR frames to the HR image should be formulated. The observed LR frames are assumed to have been produced by a degradation process that involves geometric warping, blurring, and uniform downsampling performed on the sought HR image *z* (see Fig. 2). Moreover, each LR frame is typically corrupted by additive Gaussian noise which is uncorrelated between the different LR frames. Thus, the k^{th} LR frame may be written as:

$$y_k = DBT(r_k)z_k + n_k = W(r_k)z_k + n_k \;\forall k = 1,2,3,...,K$$

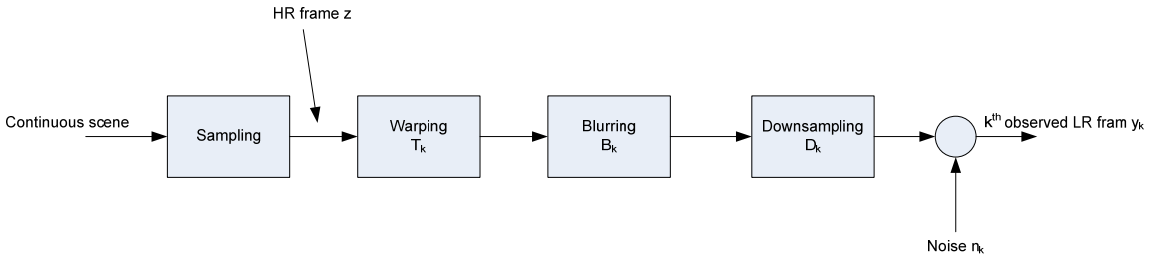

Figure 2: Block diagram of the degradation process relating each HR frame with its LR counterpart

This observation model is used to construct the unknown z image using an iterative process initialised using normalised convolution. The result is an image with higher and improved resolution in comparison with any of the originally captured images. This is demonstrated in Figure 3, where an original low resolution frame of the video sequence is shown and the constructed high resolution one using the 16 preceding frames from the video sequence. By using the previous 16 frames, any frame in the sequence (apart of course from the first 15 ones) may be upgraded this way, before further processing takes place. In combination with tracking, the method can be used to super-resolve part of the captured frame that contains the object of interest that is being tracked.

Standard Definition Frames | High Definition Frames Upsampling factor ~ 2 | Super Resolved SD Frames Upsampling factor ~ 4

Figure 3: Super resolved frames from Standard Definition Frames compared to High Definition frames

Joint Fusion and Blind Image Restoration

Image fusion is the process of combining information from different image realizations that capture the same registered scene in order to enhance the perception of the scene.

Current image fusion approaches detect salient features from the input images and fuse these details to form a new synthetic (fused) image. Image fusion approaches in can be classified into two domains:

- Spatial domain
- Transform domain

In spatial domain techniques, the input images are fused in the spatial domain using localised spatial features. The motivation to move to a transform domain is to work in a framework, where image's salient features are more clearly depicted than in the spatial domain. Transform techniques project the input images onto bases, modelling sharp and abrupt transitions (edges) and therefore represent the image into a more meaningful representation that can be used to detect and emphasize salient features, important for performing the task of the image fusion.

Image fusion is the process of combining information from different input sensor images, in order to form a new composite, synthetic image that contains all the useful information of the input images. In some cases there might be parts of the observed scene where there is only degraded information available. The task in this proposal is to identify the areas of degraded information in the input sensor images. A very simple identification approach based on local image statistics to trace the degraded areas is adopted.

Image fusion can exhibit poor performance in various situations especially when a specific region is distorted in all of the available image realizations. These distortions can be considered to be of any unknown blurring process; out-of-focus camera, motion and others. The current fusion algorithms will fuse all high quality information from the input sensors and for the common degraded areas will form a blurry mixture of the input images, as there is no high quality information available.

Imperial College are proposing a Joint Image Fusion and Restoration of overlapping areas to overcome this problem, allowing for a simultaneous reduction of additive random noise (smoothing). The question does arise: Why not restore the entire images prior to fusion?
The answer is: Restoration methods enhance edge information, but suffer from various type of distortion; ringing effects, ghost artefacts etc. This promotes the case for region based restoration, though, how can you estimate areas that are jointly distorted? This is specific to application, and should be dealt with on case by case basis. To aide estimation of overlapping areas in multi-focus case Imperial follow a very simple identification approach, based on local image statistics to trace the degraded areas.

The following algorithm for extracting these areas is used:

- Extract the edge map of the fused image f, in terms of Laplacian kernel, i.e., $\nabla^2 f(r,t)$
- Find the local standard deviations $V_L(r,t)$ for each pixel of the Laplacian edge map $\nabla^2 f(r,t)$, using 5×5 local neighbourhoods
- Reduce the dynamic range by calculating $\ln(V_L(\mathrm{r},t))$
- Estimate $V_{sL}(\mathrm{r},t)$ by smoothing $\ln(V_L(\mathrm{r},t))$ using a 15×15 median filter
- Create the common degraded area map by thresholding $V_{sL}(r,t)$ by $\mathrm{mean}_r(V_{sL}(\mathrm{r},t))-\xi$

Now an image restoration technique is applied that is based on Double weighted regularised image restoration [21] with additional robust functionals to improve the performance in the case of outliers.Blind regularised image restoration uses alternating minimisation technique based on the following function:

$$Q(h(\mathrm{r}), f(\mathrm{r})) = \underbrace{\frac{1}{2}A_1(\mathrm{r})(y(\mathrm{r}) - h(\mathrm{r}) * f(\mathrm{r}))^2}_{\text{residual}} + \underbrace{\frac{\lambda}{2}A_2(\mathrm{r})(C * f(\mathrm{r}))^2}_{\text{image regularisation}} + \underbrace{\frac{\gamma}{2}A_3(\mathrm{r})(A * h(\mathrm{r}))^2}_{\text{blur regularisation}}$$

Here residual term represents the accuracy of the restoration process. The second term – image regularisation imposes a smoothness constraint on the recovered image and the third term acts similarly to the estimated blur. Since each term of the cost function is quadratic, it can simply be optimised by applying Gradient Decent optimisation [22]. To recover the image using this cost function using the gradients of the cost function in terms of $f(r)$ and $h(r)$, the iterative scheme as follows:

- At each iteration, update:

$$f^{t+1} = f^t - \eta_1 \frac{\partial Q(h^t, f^t)}{\partial f^t}$$

$$h^{t+1} = h^t - \eta_2 \frac{\partial Q(h^t, f^{t+1})}{\partial h^t}$$

- Stop, if $\hat{f}$ and h convergence.

There terms η_1 and η_2 are the step size parameters that control the convergence rates for the image and Point Spread Function (blurring image) respectively.

Imperial College has applied robust functionals in the cost functions, in order to rectify some of the problems with using double regularisation restoration (e.g., quadratic term penalises sharp grey-level transitions resulting in blurring of image details, recovered images suffer from ringing). This results in modified original cost function:

$$Q\big(h(\mathrm{r}),\, f(\mathrm{r})\big) = \underbrace{\frac{1}{2} A_1(\mathrm{r})\rho_n\big(y(\mathrm{r}) - h(\mathrm{r}) * f(\mathrm{r})\big)^2}_{\text{residual}} + \underbrace{\frac{\lambda}{2} A_2(\mathrm{r})\rho_f\big(C * f(\mathrm{r})\big)^2}_{\text{image regularisation}} + \underbrace{\frac{\gamma}{2} A_3(\mathrm{r})\rho_d\big(A * h(\mathrm{r})\big)^2}_{\text{blur regularisation}}$$

Three distinct robust kernels, $\rho_n(\cdot)$, $\rho_f(\cdot)$ and $\rho_d(\cdot)$ are introduced in the new cost function and are referred to as the robust residual and regularising terms respectively.
Results of fusion and joint fusion and restoration are presented in Figure 11.

Multi-resolution target detection and identification

An important problem in image analysis is that of finding similar objects in sets of images, where the objects are often at different locations, scales and orientations in the various images. Partial occlusion of objects is also quite common. An effective general approach to this problem is first to find a relatively large number, typically several thousand, of key feature points in each image, and then to develop a more detailed descriptor for each keypoint. This allows points from different images to be compared and matched to create candidate pairings.

Often a reference object is taken from one image and then other instances of the object are searched for in the remaining images, so the number of reference keypoints is quite small (10 – 100), but the number of candidate keypoints can be very large (10^5 – 10^7). Hence it is important to develop keypoint descriptors which allow efficient comparison of pairs of keypoints (reference-to-candidate).

Cambridge approached the problem with the template matching technique with automatic template update. The technique produced promising results, though with this scheme the target cannot rotate arbitrarily between consecutive frames. In order to overcome this, Cambridge have adopted a technique of polar matching with dual-tree complex wavelet transform (DTCWT) coefficients.

Polar-matching with DTCWT based technique does not require the dominant orientation(s) to be computed first because it allows efficient matching of descriptor pairs in a rotationally invariant way. Polar matching matrix gives low redundant rotation invariant descriptor in addition to its computational efficiency making it very effective.

DTCWT is a multi-scale transform with decimated six subbands with complex coefficients. DTCWT is approximately shift invariant, which means that the z-transfer function, through any given subband of a forward and inverse DTCWT in tandem, is invariant to spatial shifts, and that aliasing effect due to decimation within the transform are small enough to be neglected for most image processing purposes.

Another feature of DTCWT is that the complex wavelet coefficients within any given subband are sufficiently bandlimited that it is possible to interpolate between them in order to calculate coefficients that correctly correspond to any desired sampling location or pattern of locations. Hence for a given keypoint location you may calculate the coefficients for an arbitrary sampling pattern centred on that location.

To obtain circular symmetry consistent with the subband orientations, a 13-point sampling pattern was chosen as shown in Figure 4.

The main innovation of Cambridge's work is the technique for assembling complex coefficients from the sampling locations, subband orientations, and one or more scales such that they form a 'polar' matching matrix *P*, in which a rotation of the image about the centre of the sampling pattern corresponds to a cyclic shift of the columns of *P*.

The cyclic shift property of the matrix *P*, when rotation occurs, means that Fourier transform methods are appropriate for performing correlations between two matrices P_r and P_s from the reference and search images respectively. It has been shown that this correlation may be performed efficiently in the Fourier domain, followed by a single low complexity inverse FFT to recover the correlation result as a function of rotation θ. The peak of this result is the required rotation-invariant similarity measure between P_r and P_s. A key aspect is that phase information from the complex coefficients can be fully preserved in this whole process.

The aim is to sample the directional subbands at a given scale on a grid, centred on the desired keypoint, and then to map the data to a matrix *P*, such that the rotations of the image about the keypoint are converted into linear cyclic shifts down the columns of *P*.

The sampling grid that is centred on the keypoint is shown in Figure 4. It is circularly symmetric and the sampling interval is chosen to be 30° to match that of subbands. There are 12 samples around the circle $(A, B, ..., L)$ and one at its centre *(M)*. The radius of the circle is equal to the sampling interval of the DTCWT subbands at the given scale, as this is an appropriate interval to avoid aliasing and yet provide a rich description of the keypoint locality.

Cambridge use a Bandpass interpolation technique for obtaining samples on the circular grid around each keypoint.. The information contained in a given directional complex subband is bandlimited to a particular region of 2-D frequency space, which has a centre frequency (w_1, w_2). Bandpass interpolation may be implemented by:

1. a frequency shift by $\{-w_1, -w_2\}$ down to zero frequency (i.e. a multiplication of the complex subband coefficients by $e^{[-j(w_1 x_1 + w_2 x_2)]}$ at each sampling point $\{x_1, x_2\}$),
2. a conventional lowpass Spline or bi-cubic interpolation to each new grid point,
3. inverse frequencies shift up by $\{w_1, w_2\}$ (a multiplication by $e^{[-j(w_1 y_1 + w_2 y_2)]}$ at each grid point $\{y_1, y_2\}$).

To simplify notation for the mapping to matrix *P*, for a given keypoint locality $\{A, B, ..., M\}$ in Fig. 4, the 13 subband coefficients are denoted by $\{a_d, b_d, ..., m_d\}$, where $d = 1,2,...,6$ indicates the direction of the subband. The 12×7 matrix *P* is then formed from the 13×6 coefficients and their conjugates as shown in the Matrix P.

$$P = \begin{bmatrix}
m_1 & j_1 & k_1 & l_1 & a_1 & b_1 & c_1 \\
m_2 & i_2 & j_2 & k_2 & l_2 & a_2 & b_2 \\
m_3 & h_3 & i_3 & j_3 & k_3 & l_3 & a_3 \\
m_4 & g_4 & h_4 & i_4 & j_4 & k_4 & l_4 \\
m_5 & f_5 & g_5 & h_5 & i_5 & j_5 & k_5 \\
m_6 & e_6 & f_6 & g_6 & h_6 & i_6 & j_6 \\
m_1^* & d_1^* & e_1^* & f_1^* & g_1^* & h_1^* & i_1^* \\
m_2^* & c_2^* & d_2^* & e_2^* & f_2^* & g_2^* & h_2^* \\
m_3^* & b_3^* & c_3^* & d_3^* & e_3^* & f_3^* & g_3^* \\
m_4^* & a_4^* & b_4^* & c_4^* & d_4^* & e_4^* & f_4^* \\
m_5^* & l_5^* & a_5^* & b_5^* & c_5^* & d_5^* & e_5^* \\
m_6^* & k_6^* & l_6^* & a_6^* & b_6^* & c_6^* & d_6^*
\end{bmatrix}$$

The rational for choosing this mapping can be understood from Fig. 4, which shows each of the columns of *P* in diagrammatic form using arrows on the grid of Fig. 5 to represent the direction of each subband. Hence all the samples in column 1 of *P* are taken at the midpoint *M* and correspond to the 6 subbands and their conjugates taken in sequence.

The arrow labelled '1' is from the 15° subband, arrow '2' is from the 45° subband, arrow '7' is from the conjugate of the 15° subband (i.e. the 195° subband), and so on. The circle of arrows for column 2 shows the location and subband from which each element in column 2 of *P* is taken, and this is also shown for the remaining columns. Thus you see that each column of *P* represents a particular pattern of rotationally symmetric combinations of sampling location and subband orientation, such that if an object is rotated clockwise about the centre of the sampling pattern by $k \times 30$ (*k* integer), then each column of *P* will be cyclically shifted *k* places downwards.

In order to perform rotation-invariant object detection, a matching technique is required which measures the correlation between a candidate locality in the search image and all possible rotations of a reference object in an efficient way. The Fourier transform is well-known to be a useful aid to performing cyclic correlations and in conjunction with the mapping to the *P* matrix, as above, it turns out to be effective at performing rotational correlations too. The basic idea is to form matrices $P_{r,i}$ at every keypoint *i* in the reference image, and to form matrices $P_{s,j}$ at all candidate keypoints *j* in the search image.

The pairwise correlation process for each transformed matrix pair $P_{r,i}$ and $P_{s,j}$ then becomes:

1. Multiply each Fourier component of $P_{s,j}$ with the conjugate of the equivalent Fourier component of $P_{r,i}$ to get a matrix $S_{i,j}$ ($12 \times 7 = 84$ complex multiplies).
2. Accumulate the $12 \times 7 = 84$ elements of $S_{i,j}$ into a 48 – element spectrum vector $s_{i,j}$ (84 complex adds).
3. Take the real part of the inverse FFT of $S_{i,j}$ to obtain the 48-point correlation result $s_{i,j}$ ($48 \times \log_2(48) = P_{r,i}$ 270 complexes multiply-an-adds).

There has been some concentration on the theory of Cambridge's technique, that is admittedly quite complicated, and so there is limited space for results. Cambridge has shown how rotational correlations may be performed using interpolated complex samples from the DTCWT, utilising both phase and amplitude information. There is considerable scope for extending these ideas to increase the robustness to typical image distortions (e.g. due to change of viewpoint or lighting) and small mis-registration of keypoints. Results of tracking scheme are shown in Figure 10.

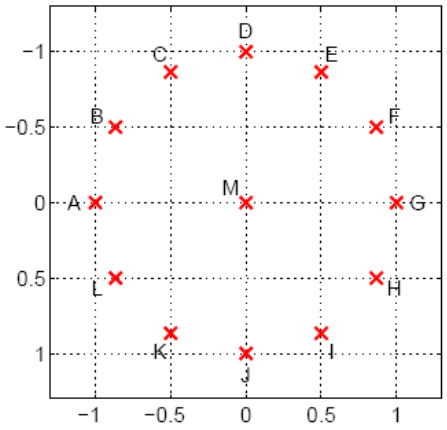

Figure 4: The 13-point circular sampling pattern for DTCWT at each keypoint location

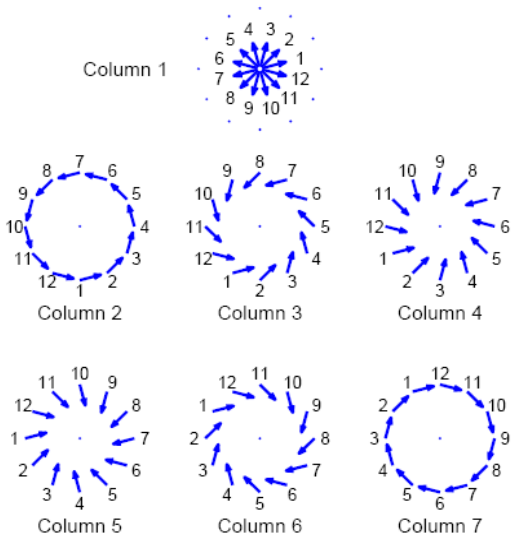

Figure 5: Shows how each column of the polar matching matrix P is comprised of a set of rotationally symmetric samples from the subbands and their conjugates, whose orientations are shown by the arrows. Numbers give the row indices in P.

Task based image and video fusion assessment

The widespread use of image fusion methods has led to a rising demand of pertinent quality assessment tools in order to compare the results obtained with different algorithms and systems or to derive an optimal setting of parameters for a specific fusion algorithm.

For man-in-the-loop applications, the performance of the fusion algorithm can be measured in terms of improvement in operator performance in different tasks like detection, recognition, classification, and tracking. This approach requires a well defined task, for which quantitative measurement can be made, and it usually involves costly and time consuming field trials.

Computational image fusion quality assessment metrics that relate to human observer performance are therefore of great value. The assessment can either be done by comparing the fused result with a reference image that provides the ground-truth, or (since such ground-truth is not available in most applications) by relating the fused result (or some of its features) to each of the input images (the so-called non-reference approach). Video fusion assessment is even more challenging as the spatio-temporal characteristics of the inputs need to be taken into account.

Previous experiments conducted at Bristol have shown that, unfortunately, subjective ranking of fused images/video and computational metric results on the one hand, and human performance for particular tasks, such as tracking, on the other hand, do not correlate well. In other words, fused images and videos that are highly ranked by computational metrics or even by human observers because of their high image quality, do not necessarily lead to improved task performance when shown to human observers.

It was thus decided to focus in the future on developing video fusion assessment metrics that correlate well with and can predict human performance for a particular task. Work on such task-dependant metrics has begun and the plan is to incorporate them into a general framework of metrics that will work for a broad range of tasks.

One of the main focuses of the AMDF Cluster project is to study the effects of resolution (SD vs. HD) and multi-sensor (visible and IR) video fusion on target tracking. Hence, it was decided to study in more detail the influence of pixel-level video fusion on object tracking using a variety of multi-sensor datasets, i.e. visible, FLIR and hyperspectral synthetic sequences from QinetiQ, visible and IR datasets from the Eden Project [9] (see Fig.6) and another visible and IR dataset available in the public domain [10]. The object tracking was done in house (in collaboration with the DIF DTC Tracking Cluster project) using several different trackers available in Bristol.

Figure 6: Tracking in an Eden sequence. Clockwise from top left the results correspond to: visible, infrared; DT-CWT fused and average fusion

The experimental results suggest strongly that on average, the IR mode is the most useful when it comes to tracking objects that are well seen in the IR spectrum. However, under some circumstances fusion is beneficial. In addition, in a situation when the task is not to simply track a single target, but to determine/estimate its position with respect to another object that is not visible in the IR video, video fusion is essential in order to perform the task successfully and accurately. This is due to the inclusion of complementary and contextual information from all input sources, making it more suitable for further analysis by either a human observer or a computer program. However, metrics for fusion assessment clearly point towards the supremacy of the multi-resolution methods, especially DT-CWT. Thus, a new, tracking-oriented, metric is needed that would be able to reliably assess the tracking performance on a fused video sequence.

Independent evaluation of the image fusion results

It is generally agreed that image fusion techniques can produce fused images that appear to be at least as good, and hopefully better than, the sum of the input parts. But *proving* how much better a fused image is over the original source images is notoriously difficult. This is essential if the additional costs of multi-sensor systems and associated processing are to be justified.

The method of assessment is greatly dependent upon the application. Empirical studies using human observers [15] have illustrated the benefits of fusion for tasks such as object detection and identification, and general situational awareness. These tasks can be performed with higher accuracy and greater confidence when compared to using the source imagery alone. Such experiments also compared grey-scale and colour fusion and concluded that the utility of colour fusion is highly dependent upon the colour mapping.

The benefits of systems whose outputs are interpreted by automatic processing algorithms (for example, target tracking) are generally easier to quantify because clearly defined metrics exist for the tasks that they perform. No equivalent standard set of metrics currently exists for fusion systems that provide imagery for human interpretation.

Part of Waterfall Solution's work is concerned with assessing the performance of image fusion schemes which provide outputs for a number of automatic tasks, principally target detection and tracking. This can be achieved by quantifying the improvement to image quality engendered by the fusion process through the use of appropriate metrics.

Measures of the quality of an image are diverse, from simple image moments (i.e. mean, standard deviation etc.) to edge densities and other image content metrics. These measures are very flexible and can therefore be chosen to match the salient image features that might be exploited - for example, a target detection algorithm.

However, single-frame image metrics are only sensitive to the contents of the current frame, and can therefore give misleading results in the presence of noise or other time-dependent image features. Metrics may also give very different results when presented with two scenes of the same quality, and so must be chosen carefully.
The sensitivity of single-frame metrics to frame content can be mitigated by normalising the metric to the results from one of the sources images to show the relative change in the metric caused by the fusion algorithm. Although this removes sensitivity to changing image content, the result is not bounded.

A novel method to visualise a potentially large number of single-frame image metrics, first proposed by Smith [16], is the polar plot (also sometimes termed Kiviat diagram when used in a control system validation context). In this representation, each normalised metric is plotted on a spoke of the polar plot along with the results for the input images so that an instantaneous comparative 'snap-shot' can be given which encompasses all metrics of interest. An example for five metrics is show below.

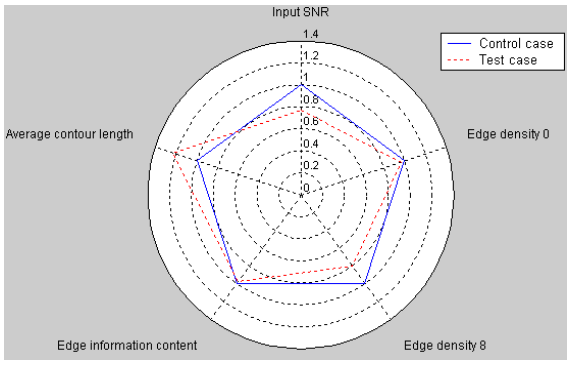

Figure 7: Polar plot representation of image metrics

Investigations have shown that single-frame image metrics can sometimes disagree with interpretation of the fused imagery by eye and some (even the more advanced) metrics may exhibit behaviour counter to task-driven measures of performance.

An alternative family of metrics is the set of image validation metrics which calculate the difference (or similarity) between two images for a given characteristic [17]. When assessing output from an image fusion technique using image validation metrics, one or more of the original input modalities is chosen as a reference. The majority of image validation metrics also have the advantage that they are automatically bounded between 0 and 1. In most cases, values approaching unity indicate that the images are nearly identical.

Examples of image validation metrics are cross-correlation, image quality, image structural similarity and peak signal-to-noise ratio. Image quality and image structural similarity metrics have both been proposed by Wang [18] et al. and the peak signal-to-noise ratio was developed by Fisher [19].

A cautionary note on the interpretation of image validation metrics is illustrated by reference to the image structural metric. A value close to 1 would indicate that the fused image has retained much of the structure of the reference input channel. However, a fused image may be of high quality but have a low score. This would occur if the fused image had retained complementary detail present in another input channel. These types of issues can be detected by running the validation metrics using each source image as the control case.

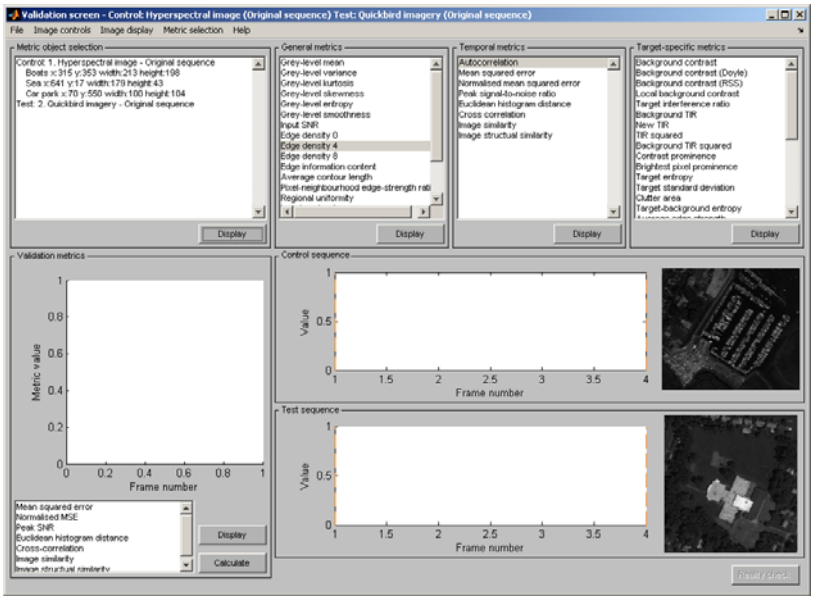

Figure 8: Screen shot of Image Analysis Tool, I2DB

The image validation metrics have equal applicability to temporal sequences in which the reference image is replaced by the previous (or next) image in the sequence. This analysis provides information on flicker and the severity of image transitions which can be a contributory factor in operator stress over long periods.

A particular family of image metrics deserving of mention are spectral metrics. The project will generate synthetic co-incident panchromatic, multi-spectral and hyperspectral imagery each at a progressively coarser resolution.

The academic teams may choose to fuse panchromatic and spectral imagery or fuse wavebands of spectral imagery. This presents a challenge in that the salient features of the data are no longer confined to two spatial dimensions but now also extend into the spectral dimension. Spectral metrics will need to be considered alongside spatial metrics in order to assess the information that has been preserved in the fusion schemes.

Image metrics - single-frame, validation, temporal and spectral – underpin any assessment of image fusion. Waterfall Solutions' integrated software tool will be used for trusted, repeatable and multi-faceted image analysis to support the assessment activities. The Figure 8 shows a screen shot of the tool.

Future Work

Hyperspectral imaging is widely used in Earth observation systems and remote sensing applications. Modern hyperspectral imaging sensors produce vast amounts of data. Thus, autonomous systems that can fuse "important" spectral bands and then classify regions of interest are required. Hyperspectral image analysis has proved useful in a variety of applications including target detection, pattern classification, material mapping and identification, etc.

At Bristol, research in this direction has focused on the development of novel algorithms for band reduction in hyperspectral images as well as for subsequent image classification. Different state-of-the-art techniques for dimensionality reduction have been investigated, which are based on entropy, mutual information and independent component analysis (ICA). New techniques based on the universal image quality index instead of entropy or mutual information have been developed and they showed considerable improvement over existing techniques.

Another important topic that is studied is how to improve the classification of hyperspectral images using image fusion techniques. The main idea is to capture the most important features and salient points of the input bands using image fusion. The information obtained using image fusion techniques can lead to improved target detection and (supervised or unsupervised) classification in hyperspectral imagery. As fusion methods relying on the dual-tree complex wavelet transform and ICA have shown to be the best performing in the multimodal image fusion, these approaches are now being generalized to work with hyperspectral image data.

Initial developments were made using the wavelet transform, which constitutes a powerful framework for implementing image fusion algorithms [5, 6]. The theoretical limits of many image fusion algorithms are determined by the underlying statistical model. Consequently, the focus was on studying prior probability models that have the potential to better characterize the different bands of hyperspectral images, as well as their associated transform coefficients.

In order to cope with more appropriate statistical model assumptions, the original weighted-average method [7] that combines images based on their local saliency was reformulated and modified. The candidate prior probability models included: generalised Gaussian distributions and alpha-stable distributions. Both were previously applied successfully to modelling natural images and were found to model the heavy-tailed image distributions more precisely than the conventional Gaussian distribution [8, 9].

Additionally, the models of image wavelet coefficients have been amended to account for both interscale dependencies and noise presence in the data. This has been achieved by incorporating bivariate shrinkage functions, derived from the underlying statistical models, into the fusion scheme. Simple and efficient implementations have been achieved with analytic estimators for special cases of the above distributions, namely the Laplace and the Cauchy distributions. In order to estimate all statistical parameters involved in the fusion algorithms a relatively novel framework that of Mellin transform theory was used.

The new method has been shown to perform very well with noisy datasets, outperforming conventional algorithms. The method has also been shown to significantly reduce the noise variance in the fused output images. Figure 9 shows an example of hyperspectral data, taken from [10], fused with the proposed method, compared to the conventional choose-max algorithm. More details on this fusion algorithm can be found in [11, 12].

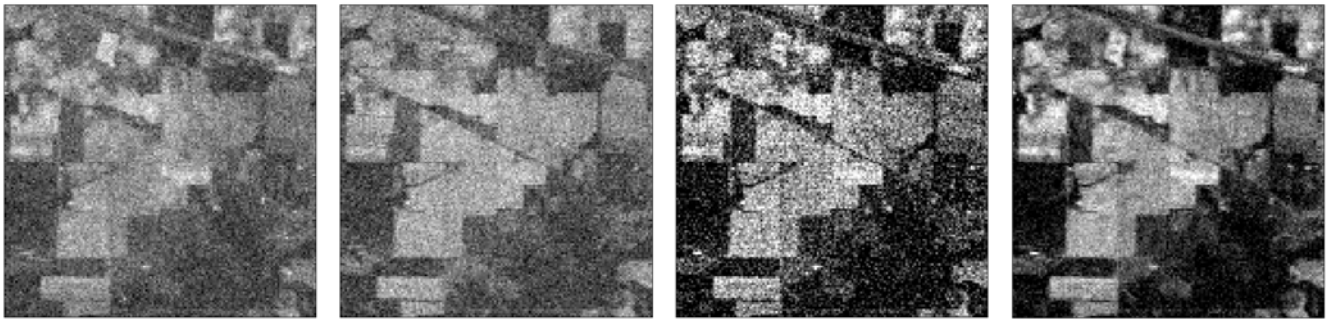

Figure 9: Statistical fusion of hyperspectral imagery, from left to right: input images from two different spectral bands, a fused image with the choose-maximum method in the wavelet domain and statistical fusion result using Laplacian modelling and bivariate shrinkage functions.

Conclusions

AMDF set out to develop academic research into applicable products. Work done to date in the area of super-resolution, joint image fusion and restoration, multi-resolution tracking and task based image fusion metric has yielded exciting results. At the same time practical issues synthetic scenario generation have been raised. This research work has revealed the weaknesses of synthetically generated video sequences; the SR research exposed the absence of sub-pixel detail within the synthetic data, whilst the stable synthetic view and ‘quiet’ simulated environment lacked the real-world occlusions and dynamically changing views of the objects, that would prove the efficacy of the new techniques. The military customer has also lamented the absence of the random fires, and high traffic densities that characterise much of the challenges in real-world surveillance data. To this effect commercial partners are working to develop new version of data set to address these issues.

Work carried out to date has shown great potential, showing convergence towards more application oriented approach. The next key stage will be to apply research to an enhanced synthetic scenario as a tool where efficacy of the research work to urban surveillance and target tracking can be proved.

References

1. http://www.multigen-paradigm.com/products/standards/openflight/index.shtml
2. N. G. Kingsbury: "Rotation-invariant local feature matching with complex wavelets", Proc. European Conference on Signal Processing (EUSIPCO), Florence, 4-8 Sept 2006
3. N. G. Kingsbury: "Complex wavelets for shift invariant analysis and filtering of signals", Journal of Applied and Computational Harmonic Analysis, vol. 10, no 3, May 2001
4. A. Katartzis and M. Petrou: "Robust Bayesian estimation and normalised convolution for super-resolution image reconstruction", British Machine Vision Conference 2007.
5. S. G. Nikolov, P. Hill, D. Bull, and N. Canagarajah: "Wavelets for image fusion," in Wavelets in Signal and Image Analysis, A. Petrosian and F. Meyer, Eds., pp. 213–244. Kluwer Academic Publishers, 2001.
6. A. M. Achim, C. N. Canagarajah, and D. R. Bull: "Complex wavelet domain image fusion based on fractional lower order moments," in Proc. of the 8th International Conference on Information Fusion, Philadelphia PA, USA, 25–29 July, 2005.
7. P. Burt and R. Kolczynski: "Enhanced image capture through fusion," in Proc. 4th International Conference on Computer Vision, Berlin 1993, pp. 173–182.
8. E. P. Simoncelli: "Modelling the joint statistics of images in the wavelet domain," in Proceedings of SPIE 44th Annual Meeting, vol. 3813, Denver, CO, USA, Jul 1999, pp. 188–195.
9. A. Achim and E. Kuruoglu: "Image denoising using bivariate-stable distributions in the complex wavelet domain," IEEE Signal Processing Letters, vol. 12, no. 1, pp. 17–20, Jan 2005.
10. Online: "Airborne visible/infrared imaging spectrometer," available at http://aviris.jpl.nasa.gov/
11. A. Loza, A. Achim, D. R. Bull, and C. N. Canagarajah: Statistical image fusion with generalized Gaussian and alpha-stable distributions. In 15th IEEE International Conference on Digital Signal Processing (DSP 2007), Cardiff, UK, July 2007 (accepted).
12. A. Achim, A. Loza, D. R. Bull, and C. N. Canagarajah: Statistical modelling for wavelet domain image fusion. In Image Fusion: Theory and Applications, T. Sthathaki Ed. Academic Press, 2007 (to appear).
13. N. Cvejic, S. G. Nikolov, H. Knowles, A. Loza, A. Achim, D. R. Bull and C. N. Canagarajah: "The Effect of Pixel-Level Fusion on Object Tracking in Multi-Sensor Surveillance Video," Workshop on Image Registration and Fusion at the IEEE Computer Society Conference on Computer Vision and Pattern Recognition, (CVPR 2007), Minneapolis, Minnesota, 23 June 2007
14. J. J. Lewis, S. G. Nikolov, A. Loza, E. Fernandez Canga, N. Cvejic, J. Li, A. Cardinali, C. N. Canagarajah, D. R. Bull, T. Riley, D. Hickman, M. I. Smith: The Eden Project multi-sensor data set, Technical report TR-UoB-WS-Eden-Project-Data-Set, University of Bristol and Waterfall Solutions Ltd, UK, 6 April 2006
15. M. Smith, J. Heather: "Review of Image Fusion Technology in 2005", Waterfall Solutions, UK; Defence and Security Symposium 2005, Orlando, 28 March - 1 April, Conference 5782: Thermosense XXVII: Thermal Image Fusion Applications
16. M. Smith: "The design, verification and validation of a generic electro-optic sensor model for system performance evaluation", PhD Thesis, University of Glasgow, UK, June 1999
17. C Angell: "Fusion Performance Using a Validation Approach", Waterfall Solutions, Information Fusion 2005, Philadelphia, 25 - 28 July
18. Wang: "Zhou Wang's Research Work", www.cns.nyu.edu/~zwang/files/research .html
19. Y Fisher et al.: "Fractal Image Compression", (Springer Verlag, 1995), section 2.4, "Pixelized Data"
20. Knutsson H &Westin C (1993). Normalized and differential convolution, *in IEEE Computer Society Conference on Computer Vision and Pattern Recognition (CVPR 93)*, New York, USA, pp. 515–523.
21. Y. L. You and M. Kaveh: "A regularisation approach to joint blur identification and image restoration." IEEE Transaction on Image Processing, 5(3):416-428, 1996
22. H. C. Andrews and B.R. Hunt: "Digital Image Restoration" Prentice-Hall 1997

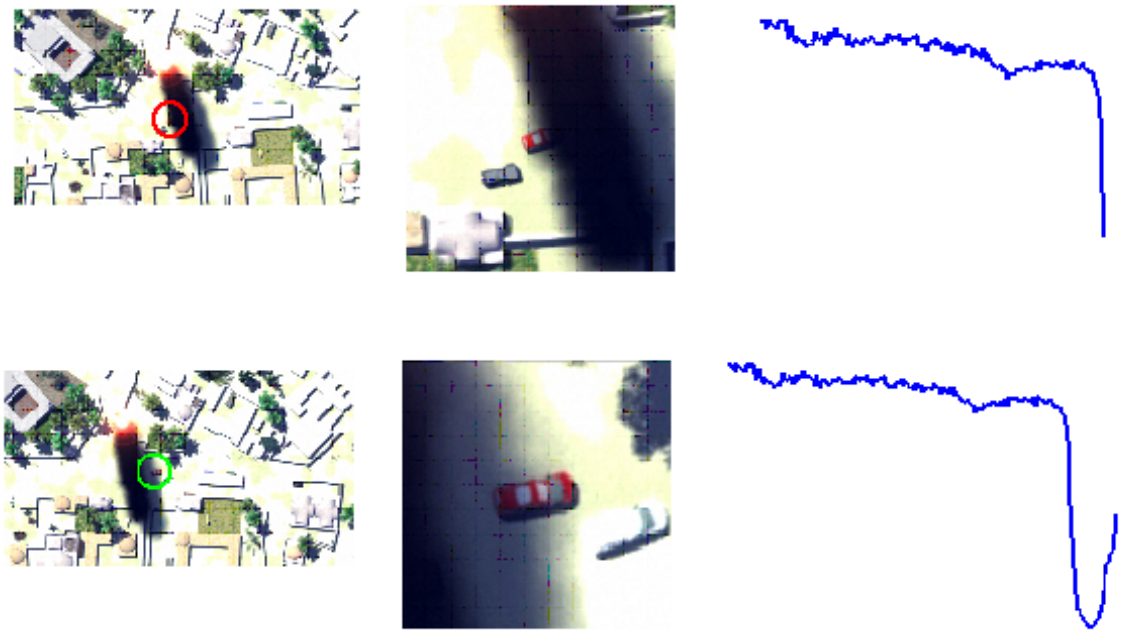

Figure 10: Tracking results with confidence level shown in red, entering and exiting occluded zone (smoke)

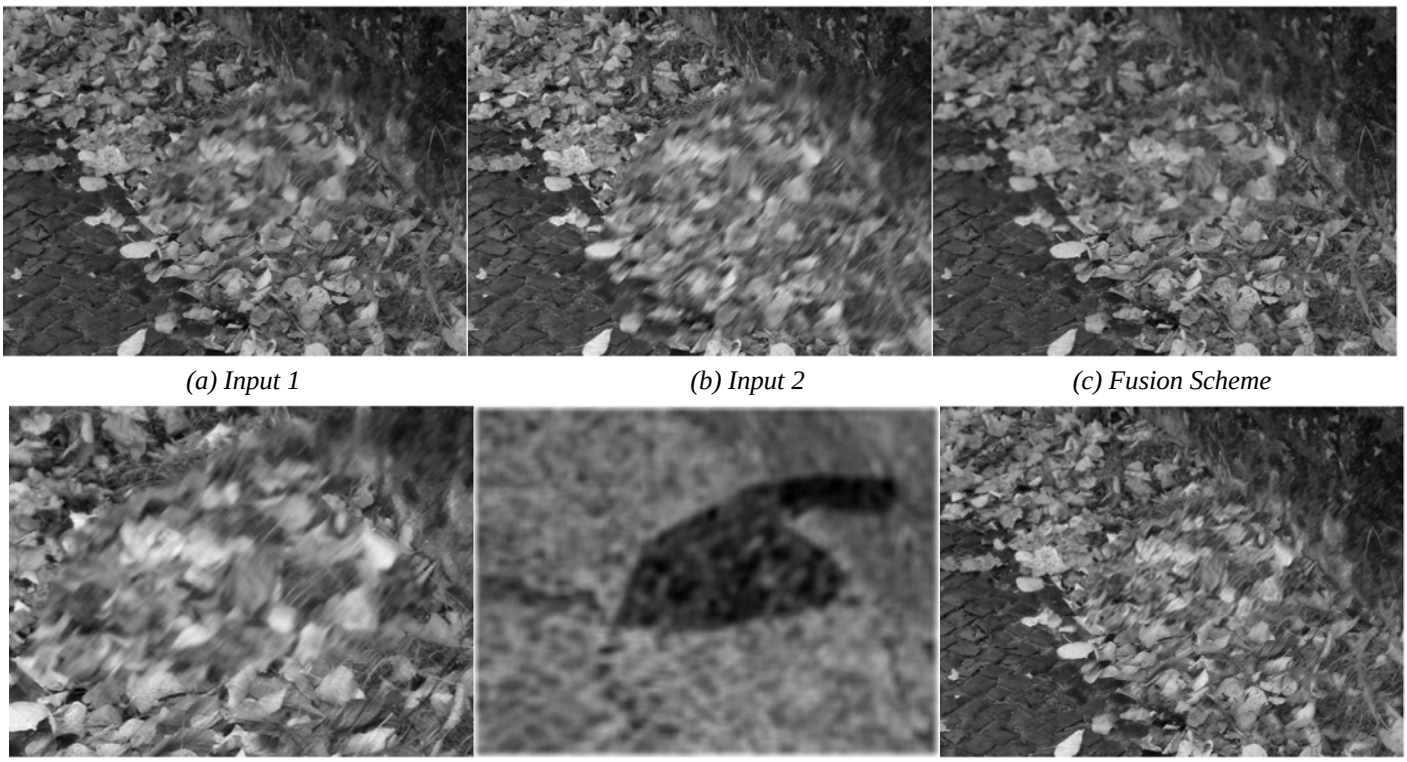

(a) Input 1 *(b) Input 2* *(c) Fusion Scheme*

(d) Common Degraded region *(e) Fusin (Affected Area)* *(f) Fusion + Restoration (Affected Area)*

Figure 11: Overall fusion improvement using the proposed fusion approach enhanced with restoration.